Electronic Supplementary Material (ESI) for Materials Chemistry Frontiers.

Precise synthesis of twins-born Fe_3O_4/FeS/Carbon nanosheet for high-rate lithium-ion battery

Linlin Ma[a], Baoxiu Hou[a], Ningzhao Shang[a], Shuaihua Zhang[a], Chun Wang[a], Lingbo Zong[d], Jianjun Song[c*], Jiangyan Wang[b*], Xiaoxian Zhao[a*]

[a] *Department of Chemistry, College of Science, Hebei Agricultural University, Baoding, 071001, China.*

[b] *State Key Laboratory of Biochemical Engineering, Institute of Process Engineering, Chinese Academy of Sciences, No. 1, Beierjie, Zhongguancun, Beijing, 100190, P. R. China.*

[c] *College of Physics, Qingdao University, Qingdao 266071, P. R. China.*

[d] *College of Chemistry and Molecular Engineering, Qingdao University of Science and Technology, Qingdao 266042, China.*

E-mail: lxzhxx@hebau.edu.cn (X, Zhao); jywang@ipe.ac.cn (J, Wang); jianjun.song@qdu.edu.cn (J, Song)

Supporting Information Caption

Figure S1: The SEM images of MIL-88b(Fe) with different citric acid added (a, no citric acid; b, 0.08 g; c, 0.05 g), and the TEM images of MIL-88b(Fe) with 0.05 g citric acid (d).

Figure S2: The SEM images of TB-FeOSC with different structure based on MIL-88b(Fe) precursor with different citric acid (a, no citric acid; b, 0.05 g citric acid; c, 0.08 g citric acid).

Figure S3: The SEM images and TEM images of TB-FeOSC-NS.

Figure S4: TG of TB-FeOSC-NS.

Figure S5: The SAED images of TB-FeOSC-NS.

Figure S6: The XRD refinement of TB-FeOSC with different temperature (a, TB-FeOSC-600; b, TB-FeOSC-NS; c, TB-FeOSC-800; d, TB-FeOSC-900) and crystal structure of Fe_3O_4 (e) and FeS (f).

Figure S7: The SEM images of TB-FeOSC with different structure (a, TB-FeOSC-600; b, TB-FeOSC-NS; c, TB-FeOSC-800; d, TB-FeOSC-900) and a scheme to synthesize TB-FeOSC at different calcination temperature (e).

Figure S8: The determination of tap density of TB-FeOSC-NS (a, volume after testing; b, quality after testing).

Figure S9: The first three CV curves of TB-FeOSC based on MIL-88b(Fe) precursor with different citric acid (a, TB-FeOSC-P; b, TB-FeOSC-NS; c, TB-FeOSC-A).

Figure S10: The galvanostatic discharge/charge curves at current densities of 0.5, 1, 2, 5, 10, 20 and 0.5 A g^{-1} of TB-FeOSC based on MIL-88b(Fe) precursor with different citric acid (a, TB-FeOSC-P; b, TB-FeOSC-NS; c, TB-FeOSC-A).

Figure S11: The BET of TB-FeOSC with different citric acid (a) and with different temperature (b).

Figure S12: The Pore size of TB-FeOSC with different citric acid (a) and with different temperature (b).

Figure S13: The CV curves at different scan rates of 0.5, 1.0, 2.0, 3.0, 4.0 and 5.0 mV s^{-1} of TB-FeOSC based on MIL-88b(Fe) precursor with different citric acid (a, TB-FeOSC-P; b, TB-FeOSC-NS; c, TB-FeOSC-A).

Figure S14: The calculation results for capacitive contribution of TB-FeOSC adjusted by citric acid. (a, TB-FeOSC-P; b, TB-FeOSC-NS; c, TB-FeOSC-A).

Figure S15: The first three CV curves of TB-FeOSC calcined at different temperature. a, TB-FeOSC-600; b, TB-FeOSC-NS; c, TB-FeOSC-800; d, TB-FeOSC-900.

Figure S16: The galvanostatic discharge/charge curves at current densities of 0.5, 1, 2, 5, 10, 20 and 0.5 A g^{-1} of TB-FeOSC calcined at different temperature. a, TB-FeOSC-600; b, TB-FeOSC-NS; c, TB-FeOSC-800; d, TB-FeOSC-900.

Figure S17: The CV curves at different scan rates of 0.5, 1.0, 2.0, 3.0, 4.0 and 5.0 mV s^{-1} of TB-FeOSC-NS calcined at different temperature. a, TB-FeOSC-600; b, TB-FeOSC-NS; c, TB-FeOSC-800; d, TB-FeOSC-900.

Figure S18: The calculation results for capacitive contribution of TB-FeOSC-NS at different temperature. (a, TB-FeOSC-600; b, TB-FeOSC-NS; c, TB-FeOSC-800; d, TB-FeOSC-900).

Figure S19: The structure of TB-FeOSC after a long circulation at a current density of 1 A g^{-1} (a1, TB-FeOSC-600; a2, TB-FeOSC-NS; a3, TB-FeOSC-800; a4, TB-FeOSC-900) and 5 A g^{-1} (a5 and a6); the S2p (b) and Fe2p (c) XPS high-resolution curves of TB-FeOSC; the XRD analysis of TB-FeOSC during circulation (d); the separator of TB-FeOSC a current density of 1 A g^{-1} (e1, TB-FeOSC-600; e2, TB-FeOSC-NS; e3, TB-FeOSC-800; e4, TB-FeOSC-900) and 5 A g^{-1} (e5).

Figure S20: The morphological and structural change of the electrode during the discharge/charge cycles.

Figure S21: The adsorption experiment of TB-FeOSC-600, TB-FeOSC-NS, TB-FeOSC-800 and TB-FeOSC-900.

Table S1: The crystal parameters and ratio of Fe_3O_4/FeS of samples treated at different temperature.

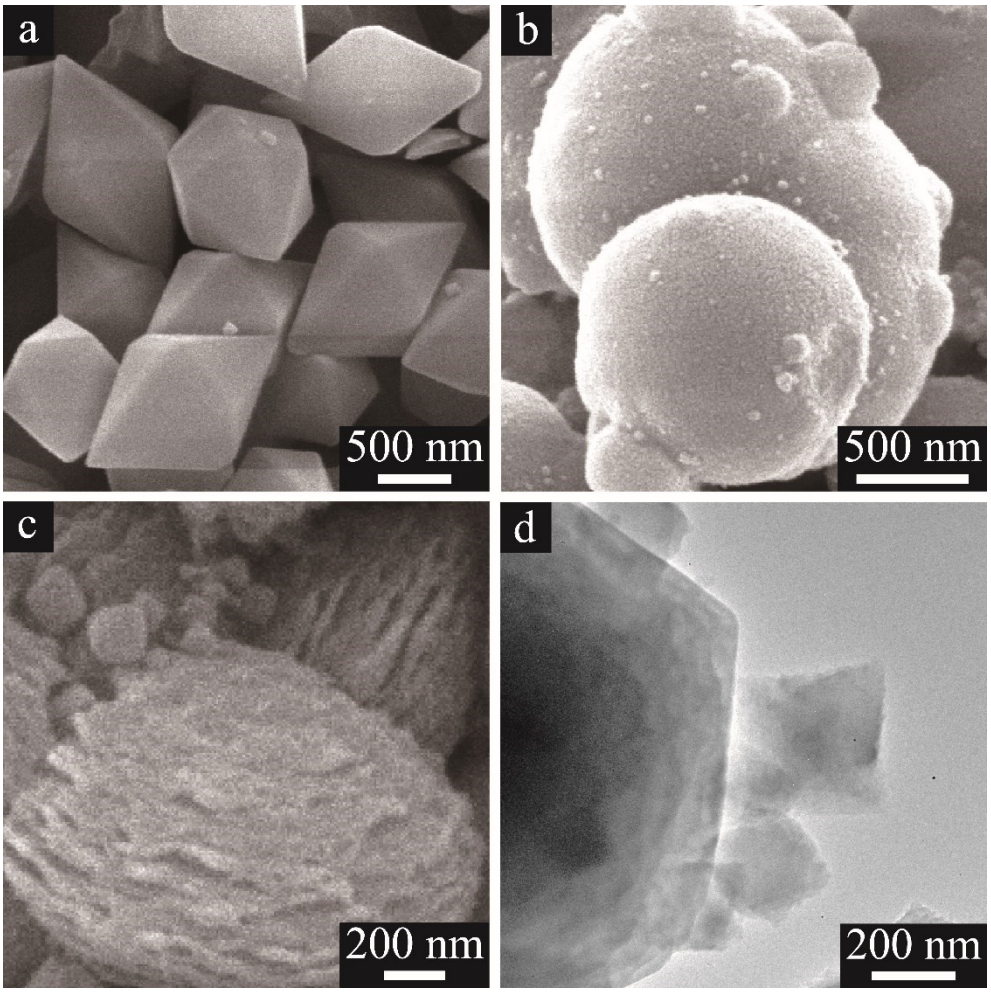

Figure S1. The SEM images of MIL-88b(Fe) with different citric acid added (a, no citric acid; b, 0.08 g; c, 0.05 g), and the TEM images of MIL-88b(Fe) with 0.05 g citric acid (d).

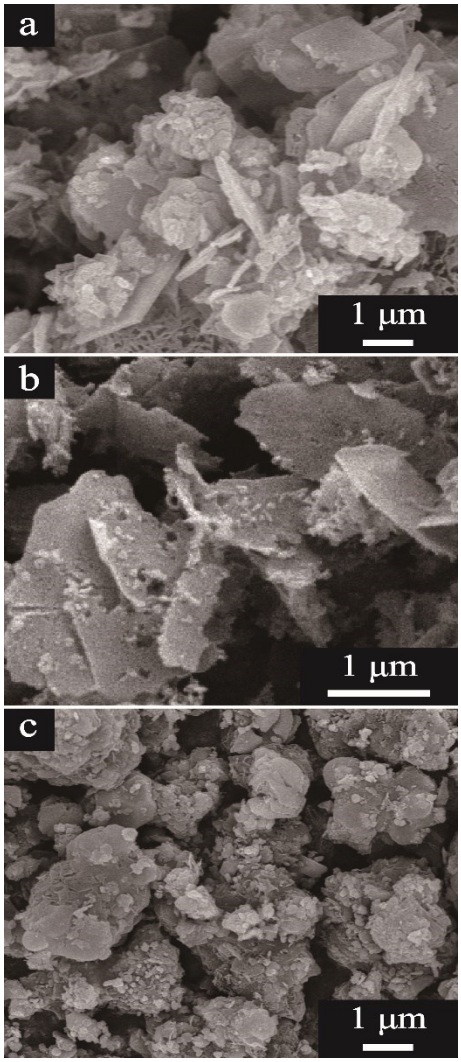

Figure S2. The SEM images of TB-FeOSC with different structure based on MIL-88b(Fe) precursor with different citric acid (a, no citric acid; b, 0.05 g citric acid; c, 0.08 g citric acid).

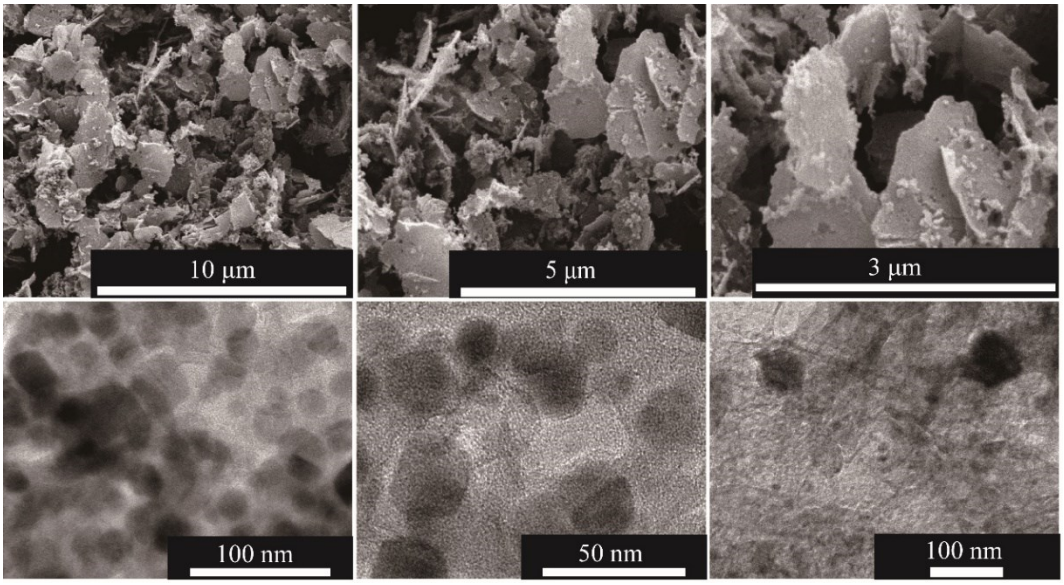

Figure S3. The SEM images and TEM images of TB-FeOSC-NS.

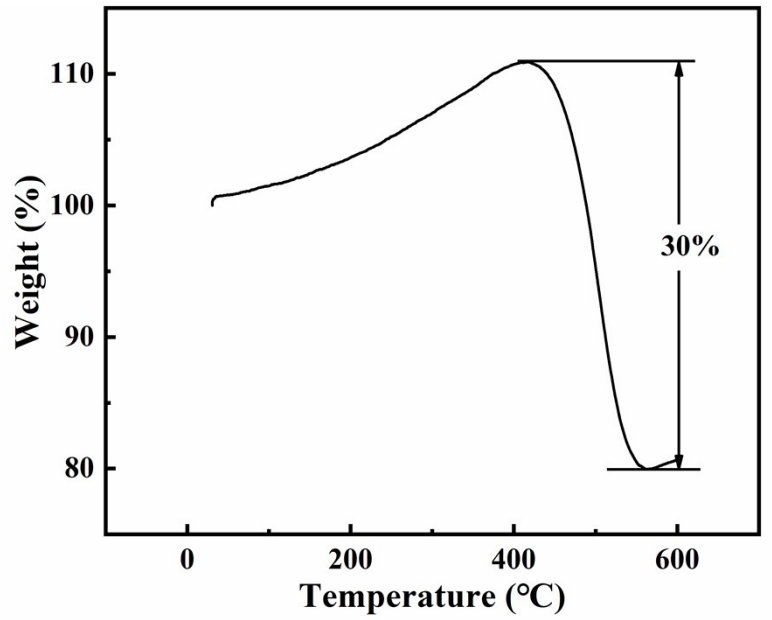

Figure S4. TG of TB-FeOSC-NS.

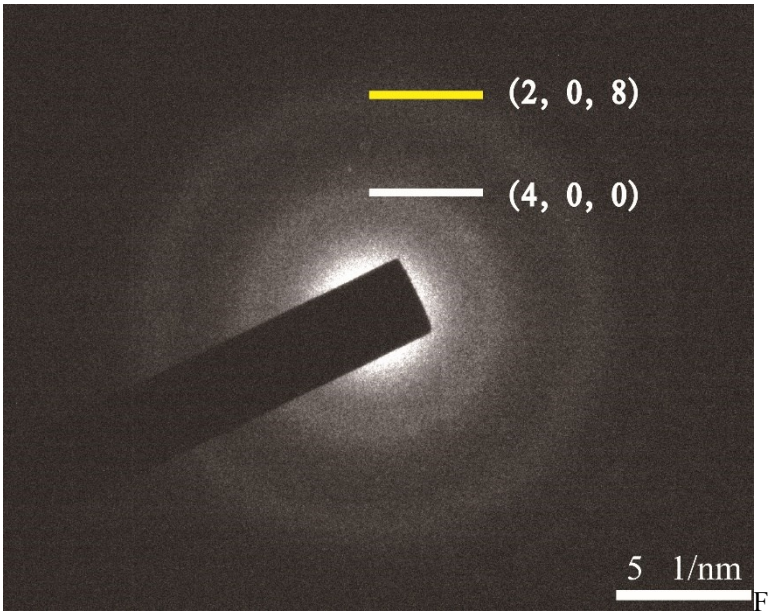

F

Figure S5. The SAED images of TB-FeOSC-NS.

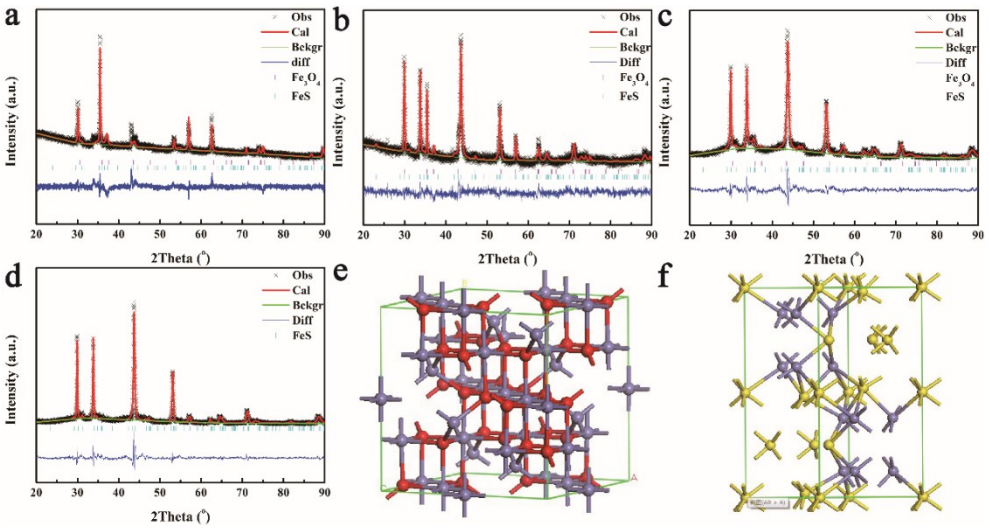

Figure S6. The XRD refinement of TB-FeOSC with different temperature (a, TB-FeOSC-600; b, TB-FeOSC-NS; c, TB-FeOSC-800; d, TB-FeOSC-900) and crystal structure of Fe_3O_4 (e) and FeS (f).

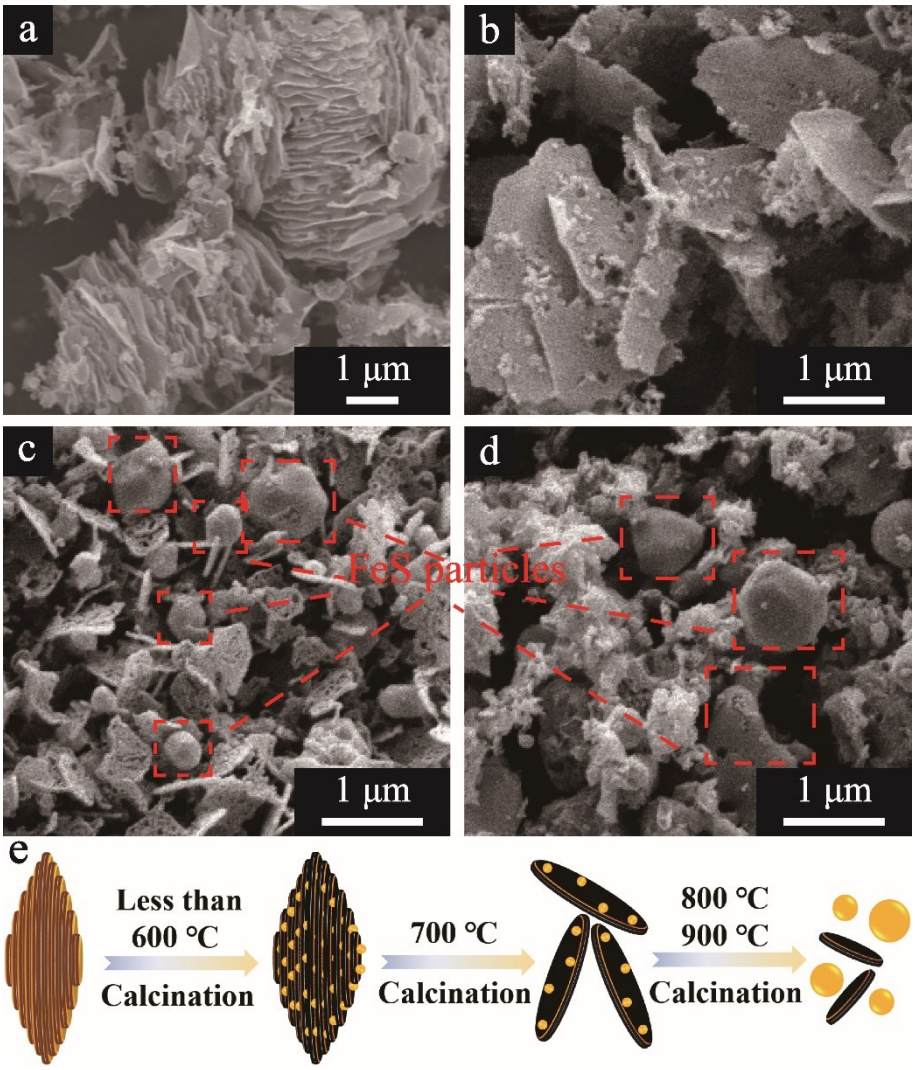

Figure S7. The SEM images of TB-FeOSC with different structure (a, TB-FeOSC-600; b, TB-FeOSC-NS; c, TB-FeOSC-800; d, TB-FeOSC-900) and a scheme to synthesize TB-FeOSC at different calcination temperature (e).

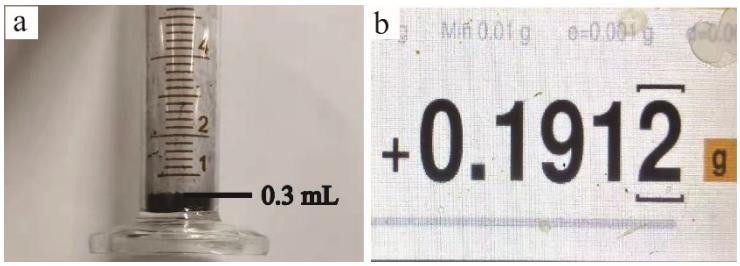

Figure S8. The determination of tap density of TB-FeOSC-NS (a, volume after testing; b, quality after testing).

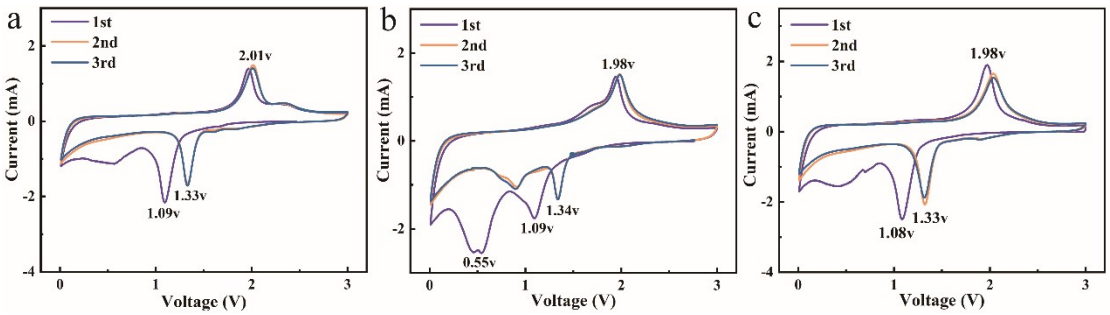

Figure S9. The first three CV curves of TB-FeOSC based on MIL-88b(Fe) precursor with different citric acid (a, TB-FeOSC-P; b, TB-FeOSC-NS; c, TB-FeOSC-A).

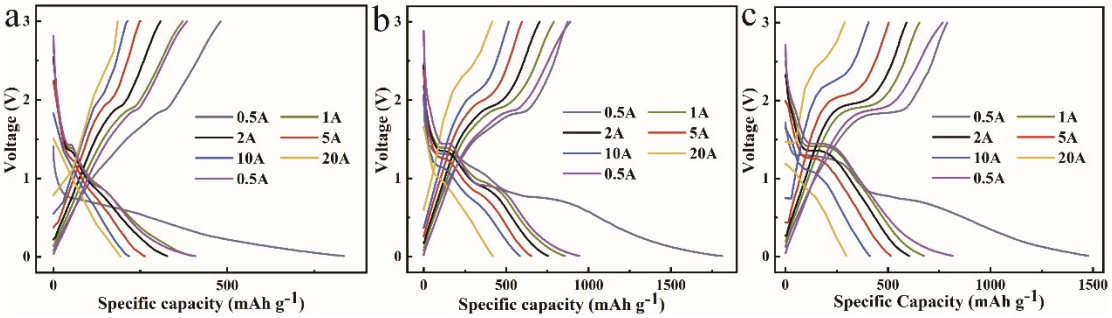

Figure S10. The galvanostatic discharge/charge curves at current densities of 0.5, 1, 2, 5, 10, 20 and 0.5 A g^{-1} of TB-FeOSC based on MIL-88b(Fe) precursor with different citric acid (a, TB-FeOSC-P; b, TB-FeOSC-NS; c, TB-FeOSC-A).

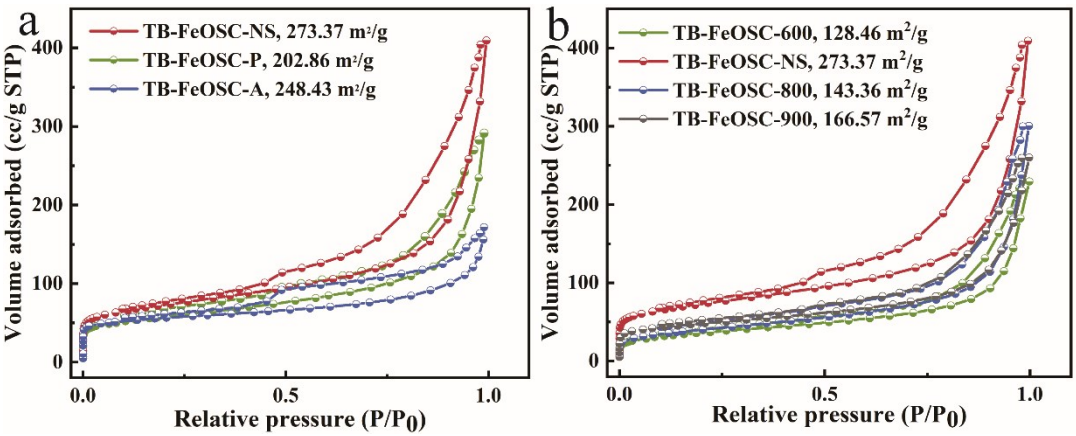

Figure S11. The BET of TB-FeOSC with different citric acid (a) and with different temperature (b).

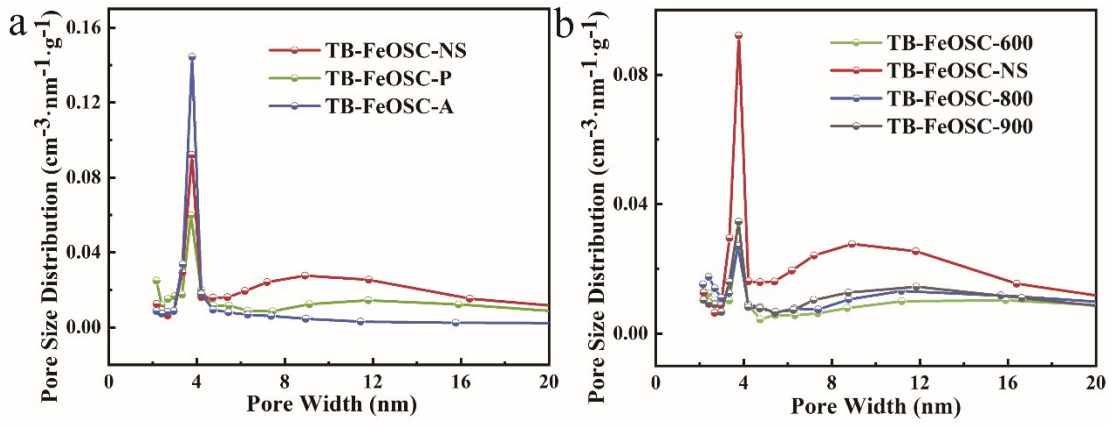

Figure S12. The pores distribution of TB-FeOSC with different citric acid (a) and different temperature (b).

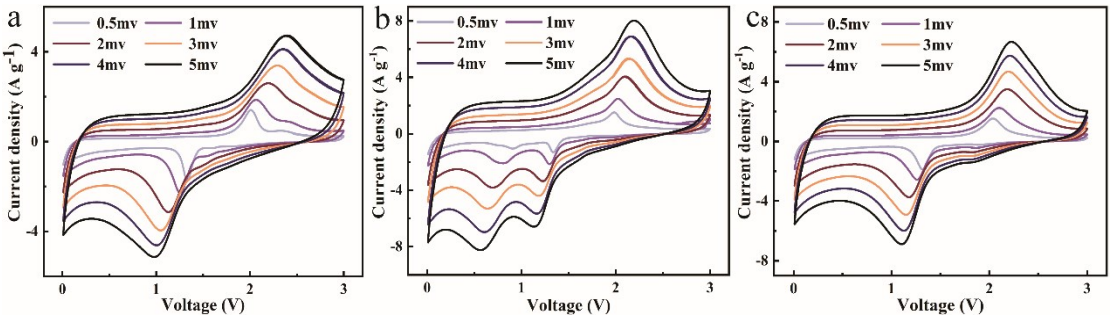

Figure S13. The CV curves at different scan rates of 0.5, 1.0, 2.0, 3.0, 4.0 and 5.0 mV s^{-1} of TB-FeOSC based on MIL-88b(Fe) precursor with different citric acid (a, TB-FeOSC-P; b, TB-FeOSC-NS; c, TB-FeOSC-A).

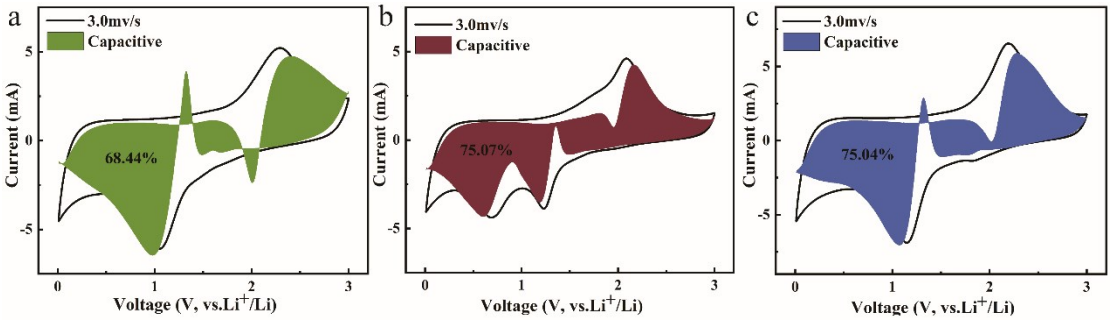

Figure S14. The calculation results for capacitive contribution of TB-FeOSC adjusted by citric acid. (a, TB-FeOSC-P; b, TB-FeOSC-NS; c, TB-FeOSC-A).

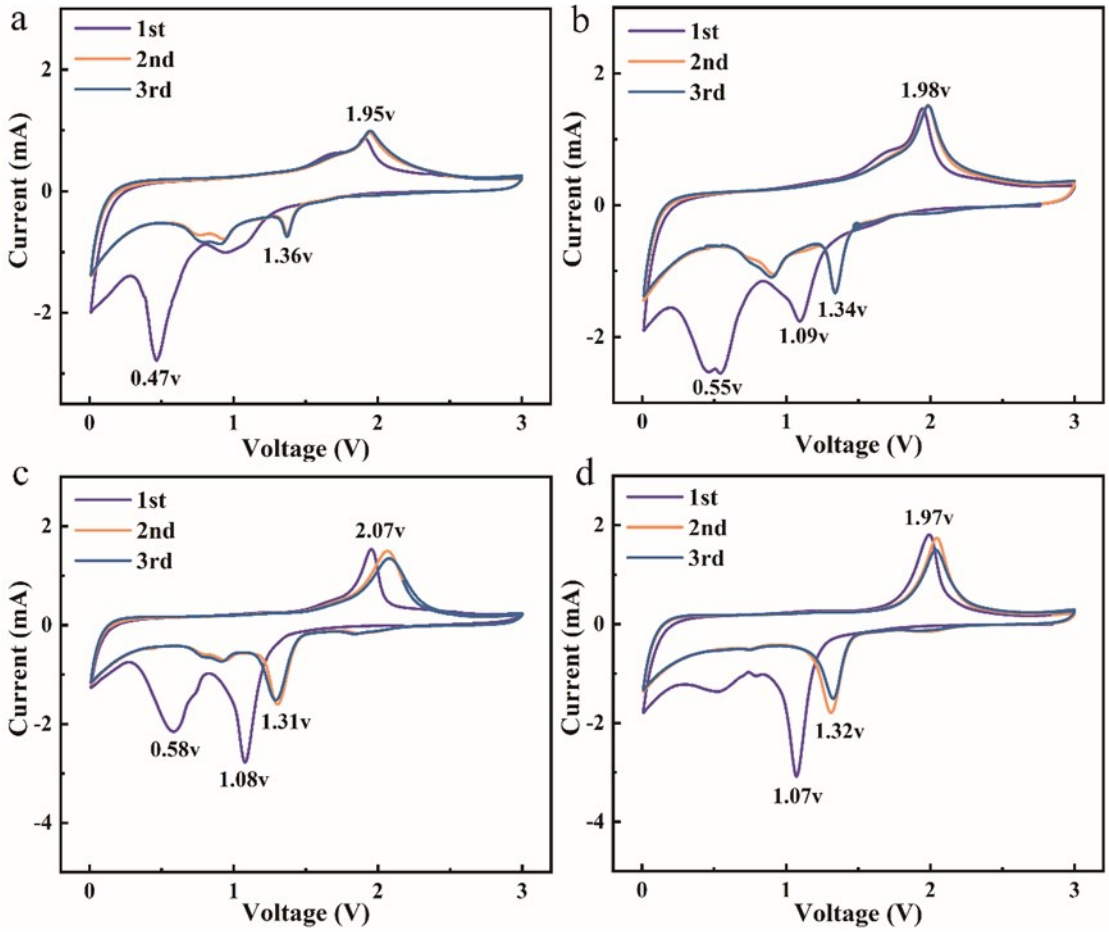

Figure S15. The first three CV curves of TB-FeOSC calcined at different temperature. a, TB-FeOSC-600; b, TB-FeOSC-NS; c, TB-FeOSC-800; d, TB-FeOSC-900.

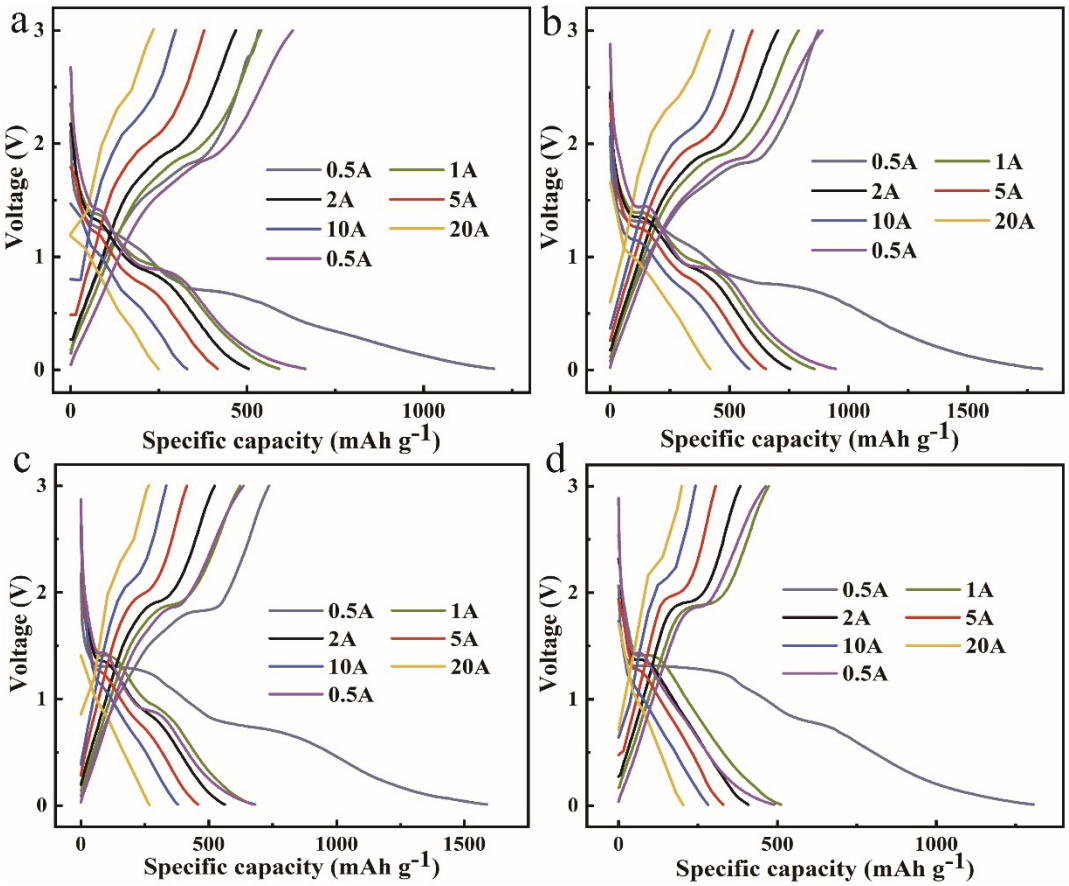

Figure S16. The galvanostatic discharge/charge curves at current densities of 0.5, 1, 2, 5, 10, 20 and 0.5 A g^{-1} of TB-FeOSC calcined at different temperature. a, TB-FeOSC-600; b, TB-FeOSC-NS; c, TB-FeOSC-800; d, TB-FeOSC-900.

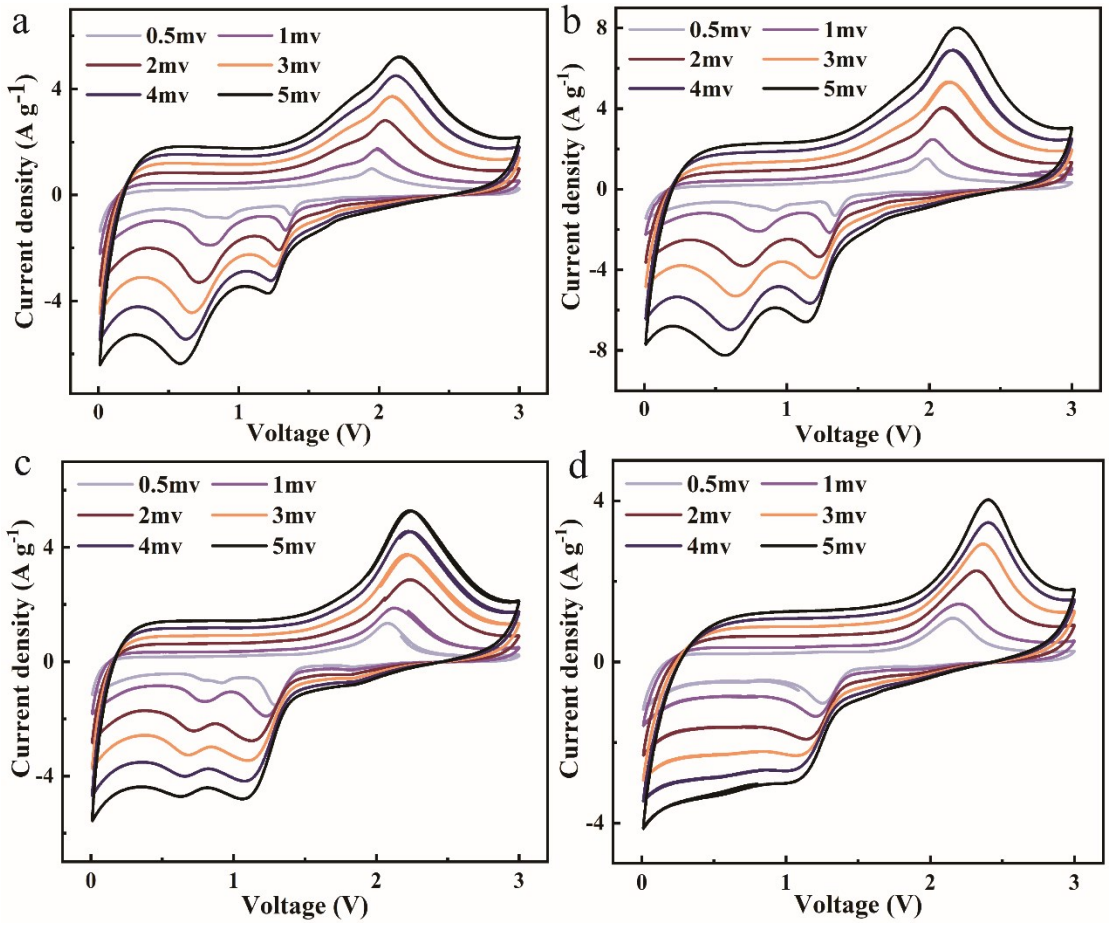

Figure S17. The CV curves at different scan rates of 0.5, 1.0, 2.0, 3.0, 4.0 and 5.0 mV s^{-1} of TB-FeOSC-NS calcined at different temperature. a, TB-FeOSC-600; b, TB-FeOSC-NS; c, TB-FeOSC-800; d, TB-FeOSC-900.

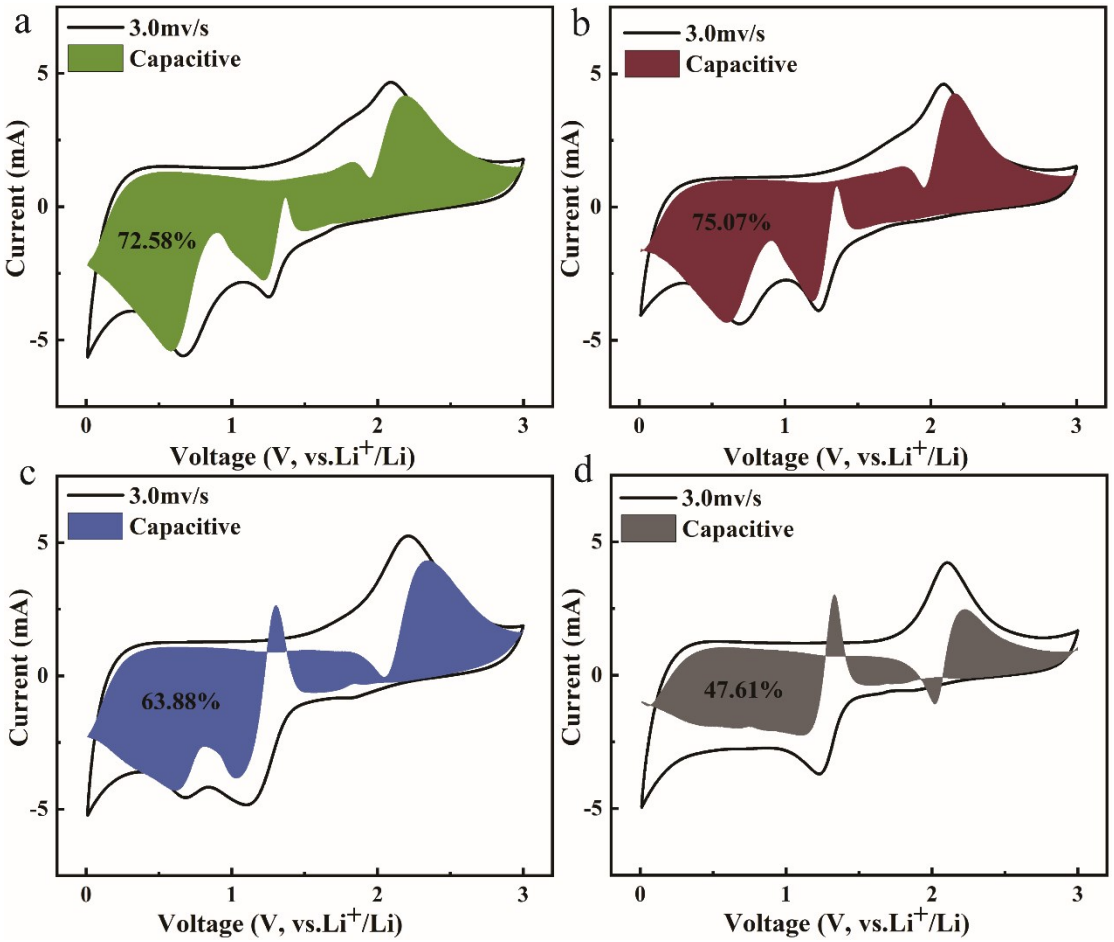

Figure S18. The calculation results for capacitive contribution of TB-FeOSC-NS at different temperature. (a, TB-FeOSC-600; b, TB-FeOSC-NS; c, TB-FeOSC-800; d, TB-FeOSC-900).

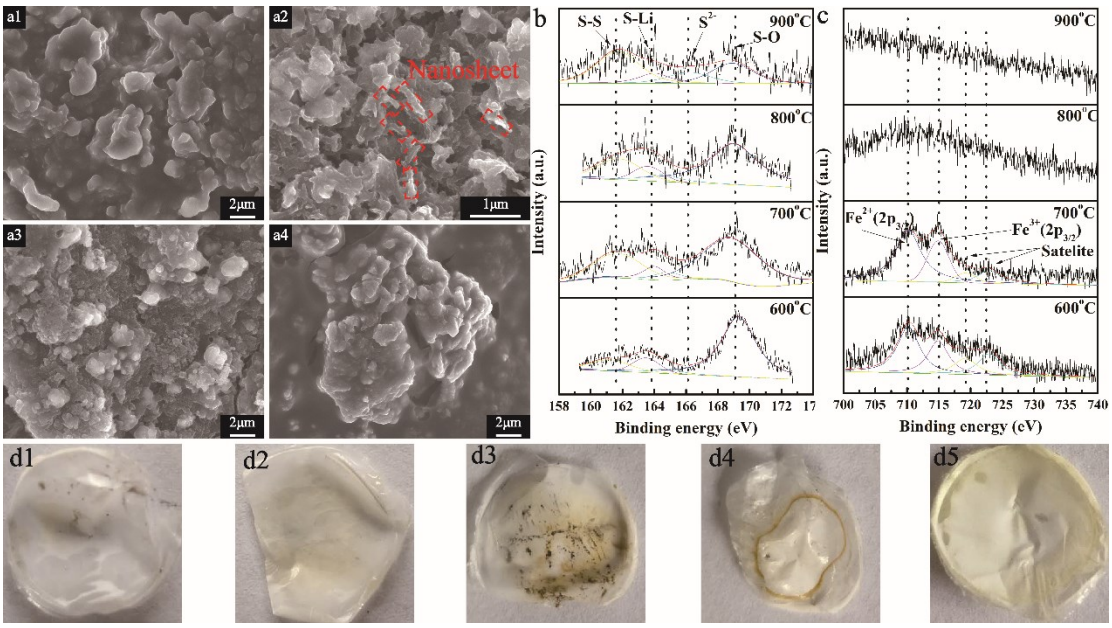

Figure S19. The structure of TB-FeOSC after a long circulation at a current density of 1 A g^{-1} (a1, TB-FeOSC-600; a2, TB-FeOSC-NS; a3, TB-FeOSC-800; a4, TB-FeOSC-900); the S2p (b) and Fe2p (c) XPS high-resolution curves of TB-FeOSC; the separator of TB-FeOSC at a current density of 1 A g^{-1} (d1, TB-FeOSC-600; d2, TB-FeOSC-NS; d3, TB-FeOSC-800; d4, TB-FeOSC-900) and 5 A g^{-1} (d5).

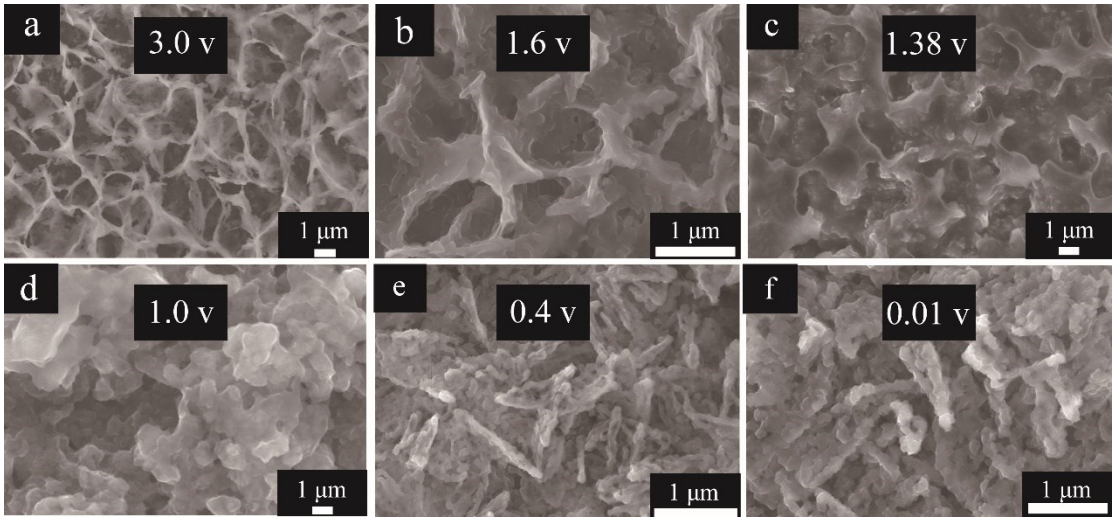

Figure S20. The morphological and structural change of the electrode during the discharge/charge cycles.

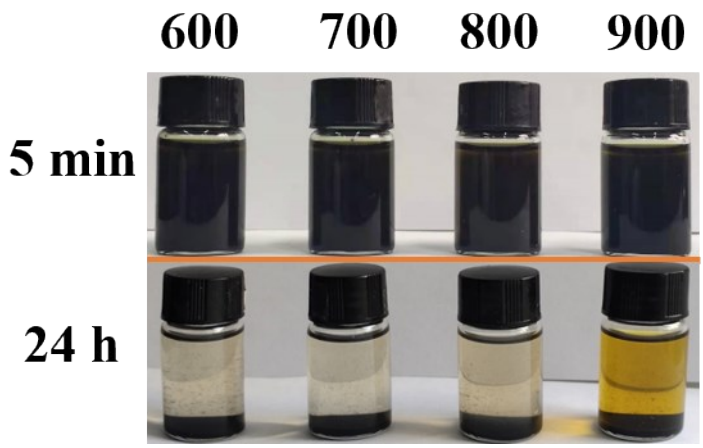

Figure S21. The adsorption experiment of TB-FeOSC-600, TB-FeOSC-NS, TB-FeOSC-800 and TB-FeOSC-900.

The TB-FeOSC-600, TB-FeOSC-NS, TB-FeOSC-800 and TB-FeOSC-900 with 20 mg were put into a bottle containing 28 μl Li_2S_6 solution of 1,3-dioxolane (DOL)/1,2-dimethoxyethane (DME) (1:1 by volume). 5 min later, all the samples were black. After 24 h later, the samples of 600 ℃, 700 ℃ were colorless, accompanying with light yellow of 800 ℃ sample, only the sample of 900 ℃ was yellow. In conclusion, the adsorption of samples treated at 600 ℃ and 700 ℃ on Li_2S_6 is stronger than 800 ℃ and 900 ℃, which further proves the stronger interaction of TB-FeOSC-NS with lithium polysulfide.

Table S1 The crystal parameters and ratio of Fe_3O_4/FeS of samples treated at different

Temperature	**600 °C**		**700 °C**		**800 °C**		**900 °C**	
	Fe_3O_4	FeS	Fe_3O_4	FeS	Fe_3O_4	FeS	Fe_3O_4	FeS
a	8.4072	5.7623	8.4117	5.9814	8.3465	5.9802	/	5.9654
b	8.4072	5.7623	8.4117	5.9814	8.3465	5.9802	/	5.9654
c	8.4072	11.721	8.4117	11.528	8.3465	11.491	/	11.468
Ratio of Fe_3O_4/FeS	1.0185/0.4334		1.5183/6.2594		1.9334/36.598		0/1	

temperature

Reference

[1] G. A. Muller, J. B. Cook, H. S. Kim, S. H. Tolbert and B. Dunn, High performance pseudo capacitor based on 2D layered metal chalcogenide nanocrystals, *Nano Lett*, 2015, **15**, 1911-1917.

[2] H. Lindström, S. Sven, S. Anita, R. Håkan, H. Johan, H. Anders and L. Sten-Eric, Li^+ ion insertion in TiO_2 (Anatase). 2. voltammetry on nanoporous films, *J. Phys. Chem. B*, 1997, **101**, 7717-7722.

[3] S. Fu, J. Ni, Y. Xu, Q. Zhang, and L. Li, Hydrogenation driven conductive $Na_2Ti_3O_7$ nanoarrays as robust binder-free anodes for sodium-ion batteries, *Nano Lett*, 2016, **16**, 4544-4551.

[4] T. Brezesinski, J. Wang, S.H. Tolbert and B. Dunn, Ordered mesoporous Alpha-MoO_3 with iso-oriented nanocrystalline walls for thin-film pseudo capacitors, *Nat. Mater*, 2010, **9**, 146-151.